Enhancing the ferromagnetic interlayer coupling between epitaxial $SrRuO_3$ layers

Lin Yang,[1,*] Lei Jin,[2] Lena Wysocki,[1] Jörg Schöpf,[1] Daniel Jansen,[1] Brajagopal Das,[3] Lior Kornblum,[3] Paul H. M. van Loosdrecht,[1] and Ionela Lindfors-Vrejoiu[1,†]

[1]*University of Cologne, Institute of Physics II, 50937 Cologne, Germany*

[2]*Ernst Ruska-Centre for Microscopy and Spectroscopy with Electrons, Forschungszentrum Jülich GmbH, 52425 Jülich, Germany*

[3]*Andrew & Erna Viterbi Department of Electrical & Computer Engineering, Technion Israel Institute of Technology, 3200003 Haifa, Israel*

(Received 2 July 2021; accepted 17 August 2021; published 27 August 2021)

Magnetic interlayer coupling is a key ingredient in designing magnetic multilayers with functionalities that reach out to the realm of applications. In epitaxial ferromagnetic (FM) oxide multilayers, the magnetic interlayer coupling is, however, less studied and its prediction is often a challenging task. Ultrathin FM $SrRuO_3$ epitaxial films with perpendicular magnetic anisotropy, interfaced with suitable oxides, may be susceptible of forming skyrmions. Hence, a strong FM interlayer coupling would be beneficial to achieve uniform switching behavior of a $SrRuO_3$-based multilayer. Previous studies reported that the coupling of two $SrRuO_3$ layers separated by a non-FM oxide spacer is at best weakly FM and the two FM layers switch at markedly different fields. Here we study the magnetic interlayer coupling between two FM $SrRuO_3$ layers separated by ultrathin $LaNiO_3$ in epitaxial heterostructures grown on $SrTiO_3(100)$ single crystals. We found that FM $SrRuO_3$ layers separated by 2 monolayers (MLs) thick $LaNiO_3$ show weak FM interlayer coupling of about 106 $\mu J/m^2$ at 10 K. The coupling becomes strongly FM for four MLs thick (about 1.6 nm) $LaNiO_3$ spacers and the two $SrRuO_3$ layers reverse their magnetization at a common value of the perpendicular magnetic field. This is likely due to a transition of the $LaNiO_3$ spacer from insulating to metallic, as its thickness increases.

DOI: 10.1103/PhysRevB.104.064444

I. INTRODUCTION

Ferromagnetic (FM) oxide thin films and multilayers, in contrast to the bare metallic FM multilayers based on Fe, Co, or Ni, have multiple tuning knobs to modify and control their physical properties. To name a few, these knobs can be the epitaxial strain imposed by the single crystalline substrate, the interactions at the coherent interfaces with dissimilar oxides, the structural modifications undergone to accommodate the mismatch of symmetry, all being often in conjunction with strong layer thickness dependence [1]. Often minute turns of the tuning knobs massively impact on the magnetic properties, such as the Curie temperature, the saturation magnetization, on the effective magnetic anisotropy and on the magneto-transport properties of the epitaxial layer. On one hand, this high sensitivity results in fascinating phenomena, such as magnetic frustration, 2D electron gases and superconductivity [2]. On the other hand, it makes it difficult to predict their occurrence, and the development of the theoretical treatment is often not keeping up with their complexity. For instance, an exciting proposal was made in 2016 that at the epitaxial interface between FM ultrathin $SrRuO_3$ layers and the large spin-orbit coupling (SOC) semimetallic $SrIrO_3$, a large interfacial Dzyaloshinskii-Moriya interaction would exist. An attractive consequence put forward was that Néel skyrmions so small as about 10 nm could form in the ultrathin $SrRuO_3$ layers [3]. Moreover, it was proposed that by applying a gate voltage across the $SrRuO_3/SrIrO_3$ bilayer, an electric field effect could be a convenient way to act on the skyrmions [4]. Stimulated by these proposals, we studied the magnetic and mangneto-transport properties of symmetric and asymmetric $SrRuO_3/SrIrO_3$ multilayers [5,6] and one aspect we addressed was the magnetic interlayer coupling [7,8]. We found that the FM $SrRuO_3$ layers are only very weakly coupled across the nonmagnetic ultrathin $SrIrO_3$ layers. The weak coupling is disadvantageous if the control of the magnetic domains is targeted. Here we report on a possible solution of how to make the magnetic interlayer coupling between two $SrRuO_3$ layers separated by a non-FM spacer strongly FM. For this purpose, we considered $LaNiO_3$, an oxide that usually does not exhibit FM ordering. The coupling between two $SrRuO_3$ layers is weakly FM for the 2 monolayers (MLs) thick $LaNiO_3$ spacer and strongly FM when the thickness of the $LaNiO_3$ spacer was increased to 4 MLs. For the latter case, the two $SrRuO_3$ layers reverse their magnetization at the same magnetic field, independent of temperature. The change of the coupling from weak to strong has to do chiefly with changes in the transport properties of the $LaNiO_3$ spacer. Bulk $LaNiO_3$ is metallic, but ultrathin $LaNiO_3$ epitaxial layers exhibit a metal-insulator transition, which typically occurs when the layers become thinner than about 4 MLs [9]. The temperature at which the transition to insulating takes place depends on the particular details such as on what substrate the layers are grown (i.e., epitaxial and symmetry conditions) and on the type and amount of defects (off-stoichiometry, oxygen content, extended structural defects) [9,10]. Moreover, a possible

*yanglin@ph2.uni-koeln.de.
†vrejoiu@ph2.uni-koeln.de.

TABLE I. Heterostructures used for the study of magnetic interlayer coupling, with the thickness of the individual $LaNiO_3$ spacer and of the two FM $SrRuO_3$ layers given in MLs (1 ML is about 0.4 nm thick). Two reference samples with a single $SrRuO_3$ layer were investigated for comparison with the heterostructure for which the strong FM coupling was observed.

Sample name	[MLs $LaNiO_3$/MLs $SrRuO_3$/MLs $LaNiO_3$/MLs $SrRuO_3$] grown on $SrTiO_3$(100)	Comment
4LNO/6SRO/4LNO/18SRO	[4/6/4/18]	Strong FM coupling
2LNO/6SRO/2LNO/18SRO	[2/6/2/18]	Weak FM coupling
[4LNO/6SRO/4LNO/18SRO]R	[4/6/4/18]	Strong FM coupling, reference sample for reproducibility of the strong FM coupling
4LNO/6SRO/4LNO	[4/6/4/0]	Reference sample to simulate the upper part of the 4LNO/6SRO/4LNO/18SRO heterostructure
4LNO/18SRO	[0/0/4/18]	Reference sample to simulate the lower part of the 4LNO/6SRO/4LNO/18SRO heterostructure

transition to antiferromagnetic (AFM) order was reported for ultrathin $LaNiO_3$ layers. Recently it was found that bulk $LaNiO_3$ also has a transition to AFM order at about 157 K, similar to the other $RNiO_3$ (R = rare earth, Y) compounds [11], after being long considered a paramagnetic material down to low temperatures. No FM order has been reported, though, for $LaNiO_3$ layers grown on $SrTiO_3$(100)-oriented substrates, such as we employ here.

II. EXPERIMENTAL DETAILS

The heterostructures studied here were grown on $SrTiO_3$(100) by pulsed-laser deposition (PLD) using a KrF excimer laser (λ = 248 nm), using the same fabrication parameters for all samples. Prior to use, all $SrTiO_3$(100) single-crystal substrates were etched in NH_4F-buffered HF for 2.5 min and annealed at 950°C for 1 h in air in order to obtain uniform TiO_2-surface termination and terraces with uniform width and one unit cell step height. The deposition temperature was 700°C and laser fluence was 3 J/cm^2 for both types of layers. The pulse repetition rate of the laser was 5 Hz for the $SrRuO_3$ layers and 1 Hz for the $LaNiO_3$ layers. For the growth of $SrRuO_3$ and $LaNiO_3$, the oxygen partial pressure was optimized at 0.133 and 0.3 mbar, respectively. The heterostructures were cooled in 100 mbar oxygen atmosphere from 700°C down to room temperature, with a rate of 10°C/min. The growth of each layer was monitored by high oxygen pressure reflective high-energy electron diffraction (RHEED). In order to study the magnetic interlayer coupling we made heterostructures in which the two $SrRuO_3$ layers had different coercive fields. We applied the same heterostructure design as we used for the study of the magnetic coupling of two layers separated by ultrathin $SrIrO_3$ [7,8]. The thickness of the top and bottom $SrRuO_3$ layers was nominally 6 and 18 MLs, respectively, and the thickness of each $LaNiO_3$ layer is nominally 2 or 4 MLs (1 ML layer is $\approx$ 0.4 nm thick). The two $SrRuO_3$ layers have different thicknesses, because here we need two layers that have different coercive fields. We make use of the fact that epitaxial $SrRuO_3$ layers have a pronounced thickness dependence of the coercive field [12–14]. A schematic of the samples is shown in Fig. 1(a). Table I summarizes the details of the main samples employed here.

The microstructure of the multilayers, such as the sharpness and the coherence of the interfaces and the uniformity of the layer thickness, was investigated by high-angle annular dark field scanning transmission electron microscopy (HAADF-STEM) on cross-section specimens. The elements distribution of the samples was characterized with energy dispersive x-ray spectroscopy (EDS) mapping. These were performed using an FEI Titan 80-200 ChemiSTEM microscope equipped with a super-X EDS system running at 200 kV. X-ray diffraction was carried out in a Rigaku SmartLab using a rotating anode source and a 2-bounce Ge(220) monochromator. Simulation of the data was done using the GlobalFit 2.0 software. The magnetization was measured with a superconducting quantum interference device (SQUID) magnetometer (MPMS XL7 from Quantum Design, magnetic field up to 7 Tesla). The surface morphology of our samples was characterized by atomic force microscopy (NX10, Park Systems). A homemade setup that enables the simultaneous measurement of linear resistance or transverse Hall resistance in van der Pauw configuration and the polar magneto-optical Kerr effect (MOKE) was used. We used copper wires glued with silver paint to the corner of the samples for the electrical measurements. We acquired simultaneously Hall resistance and Kerr rotation hysteresis loops under the same field sweeping rates of 0.3 Tesla/min. The polar MOKE studies were performed with the magnetic field applied perpendicular to the thin film surface with incoherent light from a Xe lamp. The spectrum of the polar Kerr rotation angle and its magnitude for $SrRuO_3$ crystals and epitaxial layers [15,16] are influenced by several parameters of the heterostructures, such as the layer thickness-dependent optical properties, the number of interfaces and their sharpness, and the surface morphology and its roughness [17]. Therefore, after finding the optimal measurement conditions for the Kerr rotation angle signal of each sample, we performed the MOKE investigations at slightly different wavelengths: 550 nm wavelength was used for the sample 4LNO/6SRO/4LNO/18SRO, 570 nm was used for 2LNO/6SRO/2LNO/18SRO and 4LNO/18SRO, and 520 nm was used for 4LNO/6SRO/4LNO.

III. RESULTS AND DISCUSSION

A. Microstructure investigations

We investigated the microstructure of the heterostructures with the focus on the quality of the interfaces and the

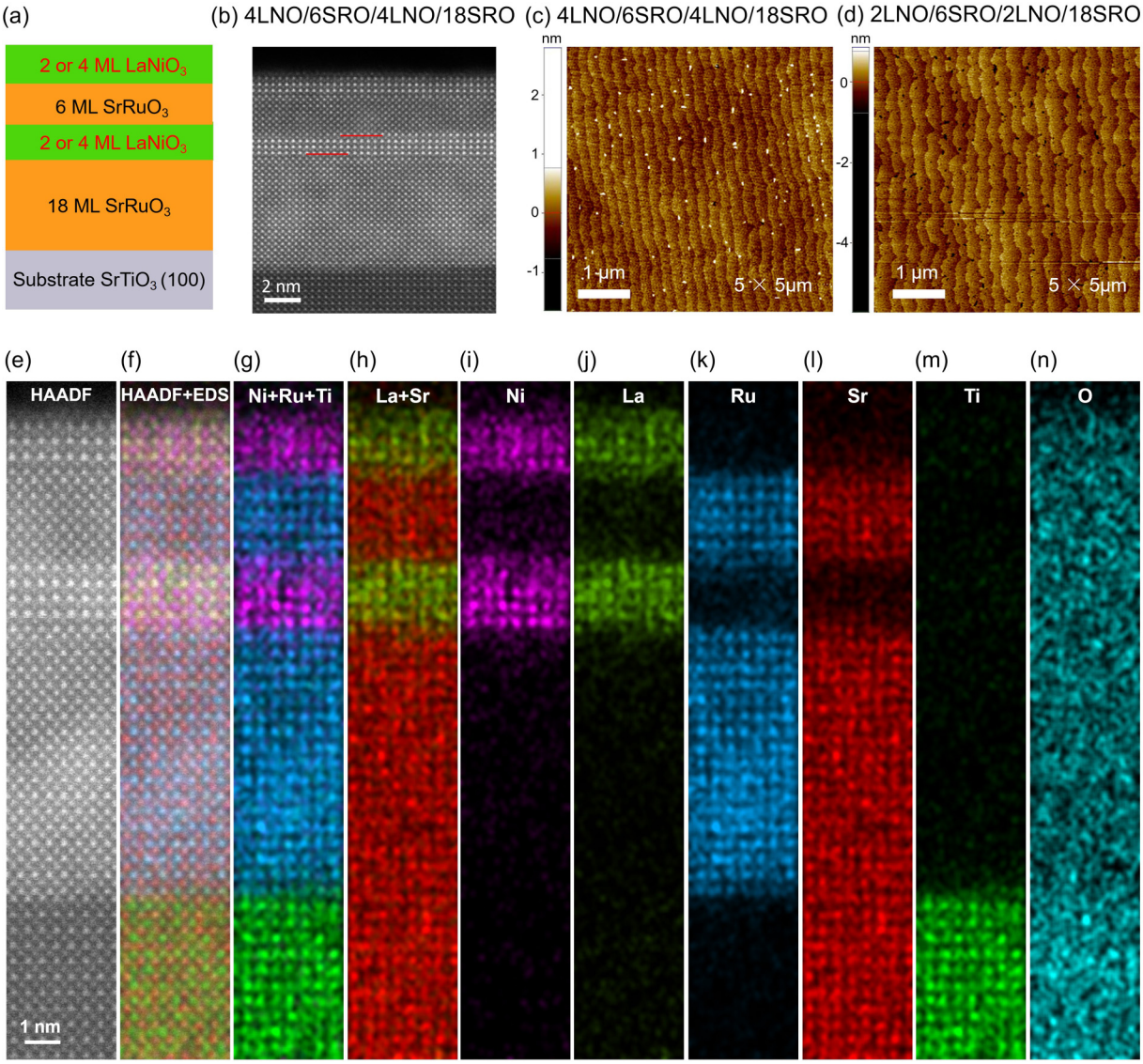

FIG. 1. The design of the heterostructures employed for the interlayer coupling study and their microstructure: (a) Schematics of samples; (b) HAADF-STEM cross-sectional image of the 4LNO/6SRO/4LNO/18SRO sample, with 4 ML $LaNiO_3$ spacer and capping layers; (c) and (d) AFM topography images (5 μm–5 μm areas) of the two main samples (as mentioned at the top of the images); (e–n) high-resolution HAADF-STEM cross-sectional image combined with EDS mapping of the distribution of the chemical elements (noted at the top of the images) across the 4LNO/6SRO/4LNO/18SRO heterostructure, including part of the $SrTiO_3$ substrate, yielding Ti signal.

integrity of the ultrathin $LaNiO_3$ spacer layer. A main concern was to ascertain that no pinholes formed in the heterostructures. Pinholes would lead to the direct connection of the two FM $SrRuO_3$ layers and result in a trivial FM coupling, which hinders the study of the intrinsic interlayer coupling through the particular type of spacer [18]. The sample that has strong FM coupling and is thus the central piece of the work, 4LNO/6SRO/4LNO/18SRO, was studied in detail by HAADF-STEM and EDS. A cross-section specimen was produced by conventional techniques, which is beneficial for $SrRuO_3$ layers that are sensitive to ion irradiation; however, slight damage of the top layer occurred and thus the top $LaNiO_3$ layer appears to be thinner than 4 MLs [see Figs. 1(b) and 1(e)]. A high magnification HAADF-STEM micrograph is shown in Fig. 1(b) and highlights the four layers of the 4LNO/6SRO/4LNO/18SRO heterostructure, with clearly separated layers of the expected thickness. Lower magnification HAADF-STEM micrographs, showing larger areas of the cross-section, are shown in the Supplemental Material (see Supplemental Fig. S2) [19]. The spacer $LaNiO_3$ layers appear to have a one ML thickness variation at the top interface with the 6 MLs $SrRuO_3$; the presence of a step is marked by the red lines drawn on the micrograph in Fig. 1(b). The chemical element distribution across the entire stack was investigated by EDS and enabled us to check the uniform distribution of the cations and the sharpness of the interfaces. Figure 1(e) shows a high magnification HAADF-STEM micrograph of the 4LNO/6SRO/4LNO/18SRO sample, marking the region where atomic resolution EDS was performed. The HAADF image overlaid with the overall EDS mapping shows an overview of the layer sequences and distribution of all the *A*-site and *B*-site perovskite-type cations [see Fig. 1(f)]. The

meaning of the colors is the same as in the elemental EDS maps shown in further detail in Fig. 1; each color corresponds to a particular ion. Taken separately, the EDS maps of the *B*-site (Ni, Ru, and Ti) and *A*-site (Sr and La) cations across the multilayer are shown in Figs. 1(g) and 1(h), respectively. Images displaying the distribution of all the individual ions (i.e., Ni, La, Ru, Sr, Ti, and O), across all the layers and at the top of the substrate, are shown in Figs. 1(i)–1(n), respectively. In conclusion, the EDS investigation strongly indicates that the spatial extent of all the cations matches the expected layer thickness, in agreement with the RHEED monitoring of the individual layer growth and fulfilling our sample design. Atomic force microscopy images of the two main heterostructures under study are shown in Figs. 1(c) and 1(d): These are topography height images of $5\,\mu\text{m} \times 5\,\mu\text{m}$ areas taken on the as-grown sample surfaces. Both samples show the step-and-terrace morphology inherent to the vicinal $SrTiO_3$ substrate. The AFM images of the 4LNO/6SRO/4LNO/18SRO heterostructure show no pinholes. For the 2LNO/6SRO/2LNO/18SRO heterostructure, the surface of the sample shows apparent tiny holes of 100–200 nm lateral size, which are about 1.8 nm deep (that is about 4.5 MLs deep) and do not reach down to the spacer layer (see Supplemental Material [19]). Thus the holes most likely do not contribute to the magnetic coupling of the two $SrRuO_3$ layers for the 2LNO/6SRO/2LNO/18SRO heterostructure.

B. Magnetic interlayer coupling

The double-layer $SrRuO_3$ heterostructures with layers of two different thicknesses were subjected to the measurement of full and minor hysteresis loops by means of MOKE and Hall effect measurements and also by SQUID magnetometry. To characterize the type and strength of coupling, we measured the major and minor hysteresis loops at different temperatures below the Curie temperatures of two different thickness of $SrRuO_3$ layers (below 140 K). In the Supplemental Material, we show the temperature dependence of the magnetization for the two heterostructures under study (see Supplemental Fig. S4) [19], from which we derived the Curie temperatures of the layers. The major and minor loops of the Kerr rotation angle measured for the 2LNO/6SRO/2LNO/18SRO heterostructure are shown in Figs. 2(a), 2(c) and 2(e). We show the results at three representative temperatures: 10, 90, and 100 K (around 100 K the anomalous Hall effect shows a change of behavior, as seen later). For comparison, we measured M(H) major and minor loops by SQUID magnetometry (see Supplemental Material, Supplemental Fig. S4) [19]. The MOKE major loops present two sharp magnetization reversal steps and tails at high magnetic field. The tail originates from the multiple magnetizations switching steps in multi-twin-domain or domain pinning in the thicker $SrRuO_3$ layer [20,21]. Additionally, the rotation of the magnetization to align with the large perpendicular magnetic field may also contribute to the tail features. Inspecting closely the loop at 10 K, we see that the two steps occur at -0.27 T corresponding to the magnetization switching of the bottom 18 MLs $SrRuO_3$ and at -0.34 T due to magnetization reversal of the top 6 MLs $SrRuO_3$. From our past investigations, we know that the two $SrRuO_3$ layers of these thicknesses have different temperature dependence of the coercive field [7]. At 10 K the 18 MLs $SrRuO_3$ has a lower coercive field, but at 90 and 100 K the thinner 6 MLs layer has a lower coercive field (as is approaching its Curie temperature of about 113 K). Similarly, two steps were observed for the Kerr loops acquired at 90 and 100 K, corresponding to two magnetization reversal processes, with the bottom $SrRuO_3$ having a larger reversal field than the top $SrRuO_3$, which is in agreement with our former work [7]. The shift of the minor Kerr rotation loops with respect to the major loops at 10, 90, and 100 K was negative and evaluated to about -100, -64, and -46 mT, respectively. The decrease of the loop shift with increasing temperature indicates a decrease of the coupling strength. For the quantitative evaluation of the coupling strength, we made use of the M(H) loop measurements by SQUID (see Supplemental Material [19]). M(H) loop measurements enabled us to determine the saturation magnetization for the two $SrRuO_3$ layers as these values are needed for the estimation of the interlayer coupling strength [7]. We estimated the interlayer coupling strength J_{IC} as 106 $\mu J/m^2$ at 10 K [22]. For the heterostructures with $SrIrO_3/SrZrO_3$ spacer, we obtained the largest FM coupling strength of about 35 $\mu J/m^2$ at 10 K [7]. Thus, the coupling of the $SrRuO_3$ layers through the 2 MLs $LaNiO_3$ spacer is FM, larger than for the $SrIrO_3/SrZrO_3$ spacer of the same thickness, however still rather weak.

When we increased the thickness of the $LaNiO_3$ spacer and capping layer to 4 MLs, a single magnetization reversal occurred at a common value of the magnetic field at all temperatures down to 10 K [see the Kerr rotation loops in Figs. 2(b), 2(d) and 2(f)]. This indicates that the 4LNO/6SRO/4LNO/18SRO heterostructure has a strong intrinsic magnetic interlayer coupling and meets our goal of finding the conditions for which the two FM layers reverse their magnetization simultaneously at the same value of the applied field. In addition, we also performed the SQUID measurements of the heterostructures as a cross-check of the Kerr rotation measurements and to measure the saturation magnetization of the $SrRuO_3$ layers, which we used in the calculation of the interlayer coupling. The SQUID M(H) and MOKE loops measurements show consistent results (see in the Supplemental Material Supplemental Fig. S4 for the comparison of such loops at 10 K) [19], confirming the strong FM coupling. A second heterostructure, [4LNO/6SRO/4LNO/18SRO]R, was made and studied by SQUID magnetometry, Kerr and Hall measurements for checking the reproducibility and further confirmed the strong FM coupling (see Supplemental Material for details) [19]. We investigated also two reference samples (see Table I) in order to get information of the properties of the single bottom 18 MLs $SrRuO_3$ layer and single top 6 MLs $SrRuO_3$ layer, when the other FM layer is not present to influence its magnetic properties. We kept the interfaces to be similar to the heterostructures, as for one reference layer we capped the 18 MLs layer with a 4 MLs $LaNiO_3$ layer (sample 4LNO/18SRO), and for the other reference we sandwiched the 6 MLs layer between two 4 MLs $LaNiO_3$ layers (sample 4LNO/6SRO/4LNO).

The Kerr rotation loops of these three reference samples are given in the Supplemental Material (see Supplemental

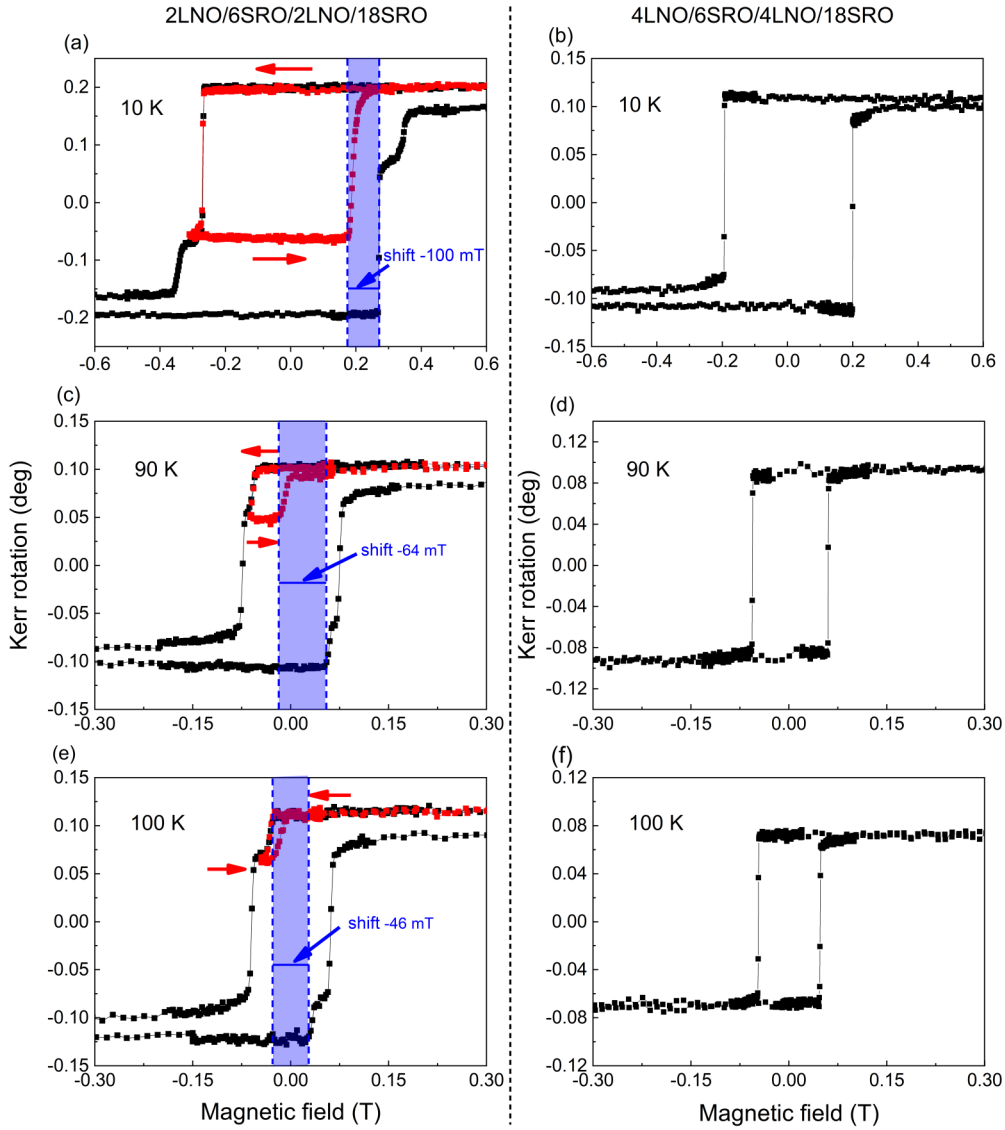

FIG. 2. MOKE (Kerr rotation) loops of the heterostructures with 2 or 4 ML thick spacer or capping $LaNiO_3$ layers: (a), (c), (e) Major loop and minor loops at 10, 90, and 100 K, respectively, for the heterostructure 2LNO/6SRO/2LNO/18SRO with weak coupling; (b), (d), and (f) only major loops for the 4LNO/6SRO/4LNO/18SRO heterostructure with strong coupling. The minor loops (marked in red) were measured between saturation in positive fields and reversal field of −0.271 T, −0.058 T, and −0.027 T. The magnetic field was applied perpendicular to the heterostructure surface for all measurements.

Figs. S5 and S6) [19]. As expected, the magnitudes of the coercive field of the two reference samples are very different: At 10 K, the magnitude is more than three times larger for the 4LNO/6SRO/4LNO. We observed that the magnitude of the coercive field of the reference sample 4LNO/18SRO is, however, very similar to that of the heterostructure 4LNO/6SRO/4LNO/18SRO. This further supports that the two $SrRuO_3$ layers are strongly coupled and this makes the coercive field of the top 6 MLs $SrRuO_3$ layer of the heterostructure decrease dramatically.

The difference in the strength of the FM coupling between the two heterostructures must be the consequence of the difference in the thickness of the $LaNiO_3$ spacer. We ascribe this to the abrupt change of the electronic properties of the $LaNiO_3$ as the thickness increases from 2 to 4 MLs [10]. The interlayer coupling is only weakly FM through the insulating 2 MLs $LaNiO_3$. For this heterostructure, the mechanism of the weak coupling can be a combination of tunneling through the insulating layer plus the effect of pinholes [7]. The coupling through the metallic 4 MLs thick $LaNiO_3$ thus becomes strongly FM, possibly via a Ruderman-Kittel-Kasuya-Yosida (RKKY) type of exchange coupling of the itinerant FM $SrRuO_3$ layers via the conduction electrons [23–27].

C. Hall effect resistance loops

Transverse resistance loops resulting from the Hall effect are a complementary way to probe the behavior of the magnetization reversal in FM thin films. Besides this, the Hall resistance loops may unravel additional features inherent to magneto-transport effects, which are not present in the M(H) loops measured by SQUID or in the Kerr rotation loops

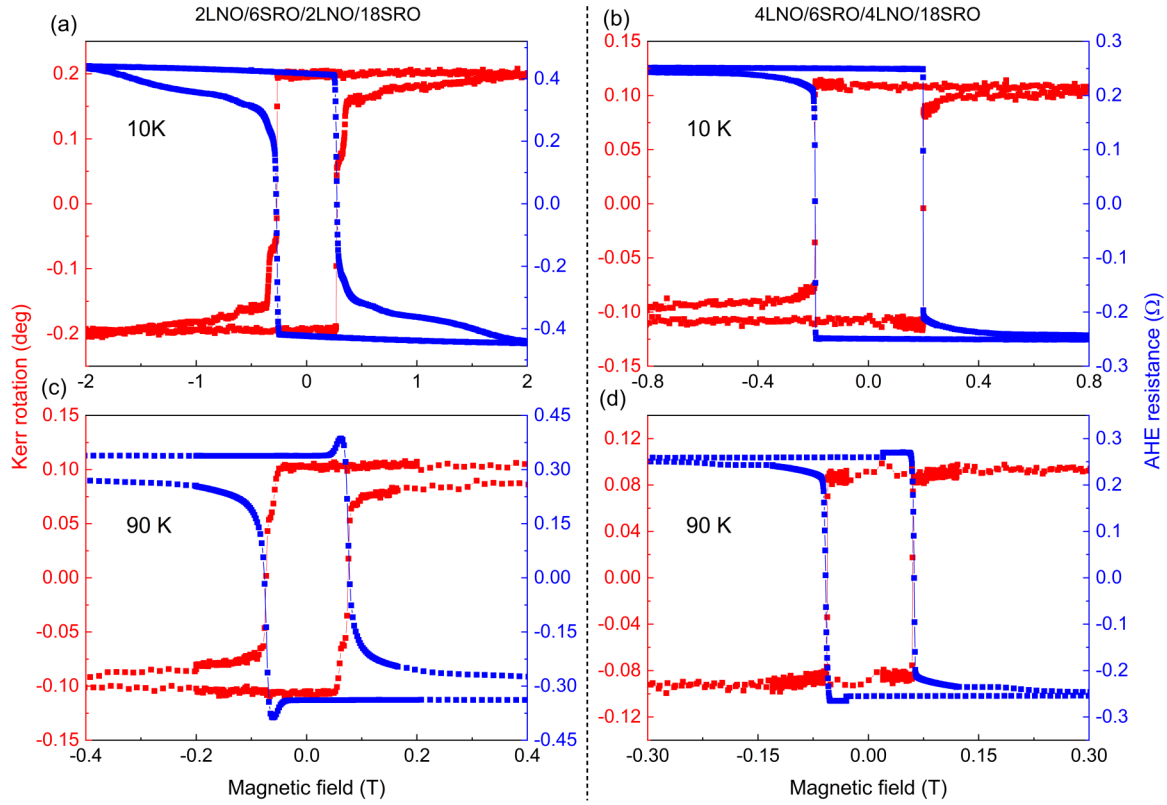

FIG. 3. Anomalous Hall resistance loops (blue) and the Kerr rotation angle loops (red) measured simultaneously at 10 and 90 K for the 2LNO/6SRO/2LNO/18SRO [(a) and (c)] and for the 4LNO/6SRO/2LNO/18SRO [(b) and (d)] heterostructures.

discussed above. Here we define the total transverse Hall resistance R_{xy} as the ratio of the Hall voltage and the excitation current I: $R_{xy} = V_{xy}/I = (V_{AHE,xy} + V_{OHE,\,xy})/I$. The measured Hall voltage, V_{xy}, has two contributions: One from the anomalous Hall effect, $V_{AHE,xy}$, and the other from the ordinary Hall effect, $V_{OHE,xy}$. The contribution of the ordinary Hall effect was subtracted from all the Hall loops shown in the paper [5,8]. We measured the Hall resistance R_{xy} of the two heterostructures in van der Pauw geometry. The MOKE and anomalous Hall effect measurements were performed simultaneously with our homebuilt setup. In Fig. 3 we show the MOKE and Hall loops measured at 10 and 90 K for the two heterostructures. Both types of loops show consistent values of the coercive field for both samples at all temperatures. The Kerr and Hall loops of both samples exhibit remarkably similar behavior at 10 K, as both the Kerr rotation angle and the Hall resistance are expected to be directly proportional to the out-of-plane magnetization. The Hall loops measured at 90 K (and at other temperatures around 90 K) have some peculiar additional features, with which we are familiar from our investigations of $SrRuO_3/SrIrO_3$ heterostructures and other recent reports [5,8,28]. Closer inspection of the Hall loop of the 2LNO/6SRO/2LNO/18SRO heterostructure in comparison to the corresponding MOKE loop [Fig.3(c)] shows that the Hall loop develops a humplike feature in the field range in which the top $SrRuO_3$ layer reverses its magnetization. We demonstrated in the past that the origin of such a hump is in the change of sign from negative to positive that the anomalous Hall effect constant undergoes as one approaches the Curie temperature, T_c, of the $SrRuO_3$ [8]. The thin top $SrRuO_3$ layer has lower T_c and thus changes its sign before the thick bottom $SrRuO_3$ layer does. The temperature dependence of the anomalous Hall constant of $SrRuO_3$ is known to be complex and it is a result of its electronic band structure [29]. In the temperature range where the two SRO layers have different signs of the anomalous Hall constant, the Hall loops have such humplike features. This is visible also for the Hall loop of the second 4LNO/6SRO/4LNO/18SRO heterostructure, though the hump is less pronounced [Fig. 3(d)]. In conclusion, the Hall effect loop measurements further support our Kerr and SQUID magnetometry loop measurements that demonstrate a strong FM interlayer coupling in the heterostructure with 4 MLs thick $LaNiO_3$ and a much weaker coupling in the heterostructure with 2 MLs $LaNiO_3$ spacer.

IV. SUMMARY

To summarize, prompted by our previous investigations of magnetic interlayer coupling for various $SrRuO_3$-based epitaxial heterostructures, we have searched for an oxide material structurally compatible with $SrRuO_3$ that can make the magnetic interlayer coupling strongly FM. Past studies with $SrTiO_3$, $SrZrO_3$, or $SrIrO_3$ used as spacers between $SrRuO_3$ layers showed that the coupling was at most weakly FM and the two FM layers reversed the magnetization at different field values [7,8]. $LaNiO_3$ turned out to be a suitable candidate and the interlayer coupling between the two $SrRuO_3$ layers changed from weakly FM to strongly FM as the thickness of the spacer increased from 2 to 4 MLs. We think that the change of the coupling strength is related to changes in the

electronic properties of the $LaNiO_3$ spacer with thickness, as it most likely becomes metallic and enables a FM coupling via a RKKY type of exchange coupling [23–27]. Finding solutions for how to couple the $SrRuO_3$ layers in a ferromagnetic manner is highly relevant for designing heterostructures in which control over the formation of the magnetic domains should be achieved.

DATA AVAILABILITY

The data that support the findings of this study are available from the corresponding author on reasonable request.

ACKNOWLEDGMENTS

We thank René Borowski and Sylvia de Waal for the etching of the STO substrates at FZ Jülich and Susanne Heijligen for assistance with SQUID measurements. I.L.-V. acknowledges the financial support from the German Research Foundation (DFG) for Project No. 403504808 within SPP2137 Skyrmionics and for Project No. 277146847 within SFB2138. We are further grateful to DFG for the financing of the purchase of the PLD-RHEED system (Project No. 407456390). L.Y. thanks the China Scholarship Council (File No.201706750015) for his fellowship. B.D. and L.K. acknowledge the support of the German Israeli Foundation for financial support (GIF Grant No. I-1510-303.10/2019).

[1] P. Zubko, S. Gariglio, M. Gabay, P. Ghosez, and J.-M. Triscone, Interface physics in complex oxide heterostructures, Annu. Rev. Condens. Matter Phys. **2**, 141 (2011).

[2] H. Hwang, Y. Iwasa, M. Kawasaki, B. Keimer, N. Nagaosa, and Y. Tokura, Emergent phenomena at oxide interfaces, Nat. Mater. **11**, 103 (2012).

[3] J. Matsuno, N. Ogawa, K. Yasuda, F. Kagawa, W. Koshibae, N. Nagaosa, Y. Tokura, and M. Kawasaki, Interface-driven topological Hall effect in $SrRuO_3$-$SrIrO_3$ bilayer, Sci. Adv. **2**, e1600304 (2016).

[4] Y. Ohuchi, J. Matsuno, N. Ogawa, Y. Kozuka, M. Uchida, Y. Tokura, and M. Kawasaki, Electric-field control of anomalous and topological Hall effects in oxide bilayer thin films, Nat. Commun. **9**, 213 (2018).

[5] L. Yang, L. Wysocki, J. Schöpf, L. Jin, A. Kovács, F. Gunkel, R. Dittmann, P. H. M. van Loosdrecht, and I. Lindfors-Vrejoiu, Origin of the hump anomalies in the Hall resistance loops of ultrathin $SrRuO_3$/$SrIrO_3$ multilayers, Phys. Rev. Materials **5**, 014403 (2021).

[6] L. Wysocki, J. Schöpf, M. Ziese, L. Yang, A. Kovács, L. Jin, R. B. Versteeg, A. Bliesener, F. Gunkel, L. Kornblum, R. Dittmann, P. H. M. van Loosdrecht, and I. Lindfors-Vrejoiu, Electronic inhomogeneity influence on the anomalous Hall resistivity loops of $SrRuO_3$ epitaxially interfaced with 5*d* perovskites, ACS Omega **5**, 5824 (2020).

[7] L. Wysocki, R. Mirzaaghayev, M. Ziese, L. Yang, J. Schöpf, R. B. Versteeg, A. Bliesener, J. Engelmayer, A. Kovács, L. Jin, F. Gunkel, R. Dittmann, P. H. M. van Loosdrecht, and I. Lindfors-Vrejoiu, Magnetic coupling of ferromagnetic $SrRuO_3$ epitaxial layers separated by ultrathin non-magnetic $SrZrO_3$/$SrIrO_3$, Appl. Phys. Lett. **113**, 192402 (2018).

[8] L. Wysocki, L. Yang, F. Gunkel, R. Dittmann, P. H. M. van Loosdrecht, and I. Lindfors-Vrejoiu, Validity of magnetotransport detection of skyrmions in epitaxial $SrRuO_3$ heterostructures, Phys. Rev. Materials **4**, 054402 (2020).

[9] M. Golalikhani, Q. Lei, R. Chandrasena, L. Kasaei, H. Park, J. Bai, P. Orgiani, J. Ciston, G. Sterbinsky, D. Arena, P. Shafer, E. Arenholz, B. Davidson, A. Millis, A. Gray, and X. Xi, Nature of the metal-insulator transition in few-unit-cell-thick $LaNiO_3$ films, Nat. Commun. **9**, 2206 (2018).

[10] S. Catalano, M. Gibert, J. Fowlie, J. Íñiguez, J.-M. Triscone, and J. Kreisel, Rare-earth nickelates $RNiO_3$: thin films and heterostructures, Rep. Prog. Phys. **81**, 046501 (2018).

[11] H. Guo, Z. Li, L. Zhao, Z. Hu, C. Chang, C. Kuo, W. Schmidt, A. Piovano, T. Pi, O. Sobolev, D. Khomskii, L. Tjeng, and A. Komarek, Antiferromagnetic correlations in the metallic strongly correlated transition metal oxide $LaNiO_3$, Nat. Commun. **9**, 43 (2018).

[12] J. Xia, W. Siemons, G. Koster, M. R. Beasley, and A. Kapitulnik, Critical thickness for itinerant ferromagnetism in ultrathin films of $SrRuO_3$, Phys. Rev. B **79**, 140407(R) (2009).

[13] G. Koster, L. Klein, W. Siemons, G. Rijnders, J. S. Dodge, C.-B. Eom, D. H. A. Blank, and M. R. Beasley, Structure, physical properties, and applications of $SrRuO_3$ thin films, Rev. Mod. Phys. **84**, 253 (2012).

[14] G. Malsch, D. Ivaneyko, P. Milde, L. Wysocki, L. Yang, P. H. van Loosdrecht, I. Lindfors-Vrejoiu, and L. M. Eng, Correlating the nanoscale structural, magnetic, and magneto-transport properties in $SrRuO_3$-based perovskite thin films: Implications for oxide skyrmion devices, ACS Appl. Nano Mater. **3**, 1182 (2020).

[15] H. Ohta, E. Kulatov, J. S. Dodge, Yu. Uspenskii, and S. Halilov, Optics and magneto-optics of $SrRuO_3$, J. Magn. Soc. Jpn. **22**, S2-185 (1998).

[16] R. B. Versteeg, Optically probed order and dynamics in the chiral cluster magnet Cu_2OSeO_3, Ph.D. thesis, Universität zu Köln, 2019.

[17] M. Veis, M. Zahradnik, R. Antos, S. Visnovsky, P. Lecoeur, D. Esteve, S. Autier-Laurent, j-p Renard, and P. Beauvillain, Interface effects and the evolution of ferromagnetism in $La_{2/3}Sr_{1/3}MnO_3$ ultrathin films, Sci. Technol. Adv. Mater. **15**, 015001 (2014).

[18] J. F. Bobo, H. Kikuchi, O. Redon, E. Snoeck, M. Piecuch, and R. L. White, Pinholes in antiferromagnetically coupled multilayers: Effects on hysteresis loops and relation to biquadratic exchange, Phys. Rev. B **60**, 4131 (1999).

[19] See Supplemental Material at http://link.aps.org/supplemental/10.1103/PhysRevB.104.064444 for additional microstructure investigations, additional SQUID magnetization (temperature and field dependence) data, and for MOKE loop measurements of all the relevant samples, which includes additionally Refs. [30–32].

[20] V. Jeudy, R. Díaz Pardo, W. Savero Torres, S. Bustingorry, and A. B. Kolton, Pinning of domain walls in thin ferromagnetic films, Phys. Rev. B **98**, 054406 (2018).

[21] W. Wang, L. Li, J. Liu, B. Chen, Y. Ji, J. Wang, G. Cheng, Y. Lu, G. Rijnders, G. Koster, W. Wu, and Z. Liao, Magnetic domain engineering in $SrRuO_3$ thin films, Npj Quantum Mater. **5**, 73 (2020).

[22] P. A. A. van der Heijden, P. J. H. Bloemen, J. M. Metselaar, R. M. Wolf, J. M. Gaines, J. T. W. M. van Eemeren, P. J. van der Zaag, and W. J. M. de Jonge, Interlayer coupling between Fe_3O_4 layers separated by an insulating nonmagnetic MgO layer, Phys. Rev. B **55**, 11569 (1997).

[23] P. Bruno and C. Chappert, Oscillatory Coupling between Ferromagnetic Layers Separated by a Nonmagnetic Metal Spacer, Phys. Rev. Lett. **67**, 1602 (1991).

[24] J. Unguris, R. J. Celotta, and D. T. Pierce, Observation of Two Different Oscillation Periods in the Exchange Coupling of Fe/Cr/Fe(100), Phys. Rev. Lett. **67**, 140 (1991).

[25] Q. Leng, V. Cros, R. Schäfer, A. Fuss, P. Grünberg, and W. Zinn, Interlayer coupling across noble metal spacers, J. Magn. Magn. Mater. **126**, 367 (1993).

[26] M. Stiles, Interlayer exchange coupling, J. Magn. Magn. Mater. **200**, 322 (1999).

[27] N. M. Kreines, Investigation of interlayer coupling in $[Fe/Cr]_n$ magnetic multilayer structures by the ferromagnetic resonance method (review), Low Temp. Phys. **28**, 581 (2002).

[28] T. C. van Thiel, D. J. Groenendijk, and A. D. Caviglia, Extraordinary Hall balance in ultrathin $SrRuO_3$ bilayers, J. Phys.: Mater. **3**, 025005 (2020).

[29] L. Klein, J. R. Reiner, T. H. Geballe, M. R. Beasley, and A. Kapitulnik, Extraordinary Hall effect in $SrRuO_3$, Phys. Rev. B **61**, R7842(R) (2000).

[30] J. Choi, C. B. Eom, G. Rijnders, H. Rogalla, and D. H. A. Blank, Growth mode transition from layer by layer to step flow during the growth of heteroepitaxial $SrRuO_3$ on (001) $SrTiO_3$, Appl. Phys. Lett. **79**, 1447 (2001).

[31] K. Tsubouchi, I. Ohkubo, H. Kumigashira, Y. Matsumoto, T. Ohnishi, M. Lippmaa, H. Koinuma, and M. Oshima, Epitaxial growth and surface metallic nature of $LaNiO_3$ thin films, Appl. Phys. Lett. **92**, 262109 (2008).

[32] C. L. Platt, M. R. McCartney, F. T. Parker, and A. E. Berkowitz, Magnetic interlayer coupling in ferromagnet/insulator/ferromagnet structures, Phys. Rev. B **61**, 9633 (2000).